NANO LETTERS
Letter
Cite This: Nano Lett. 2018, 18, 6974−6980
pubs.acs.org/NanoLett

Defect Manipulation To Control ZnO Micro-/Nanowire-Metal Contacts

Jonathan W. Cox,[†] Geoffrey M. Foster,[‡] Alexander Jarjour,[§] Holger von Wenckstern,[∥] Marius Grundmann,[∥] and Leonard J. Brillson*[,†,‡]

[†]Department of Electrical and Computer Engineering, The Ohio State University, 205 Dreese Lab, 2015 Neil Avenue, Columbus, Ohio 43210, United States

[‡]Department of Physics, Ohio State University, 191 W. Woodruff Avenue, Columbus, Ohio 43210, United States

[§]Department of Physics, Cornell University, 171 Clark Hall, Ithaca, New York 14850, United States

[∥]Institut für Experimentelle Physik II, Universität Leipzig, Linnéstrasse 5, 04103 Leipzig, Germany

Supporting Information

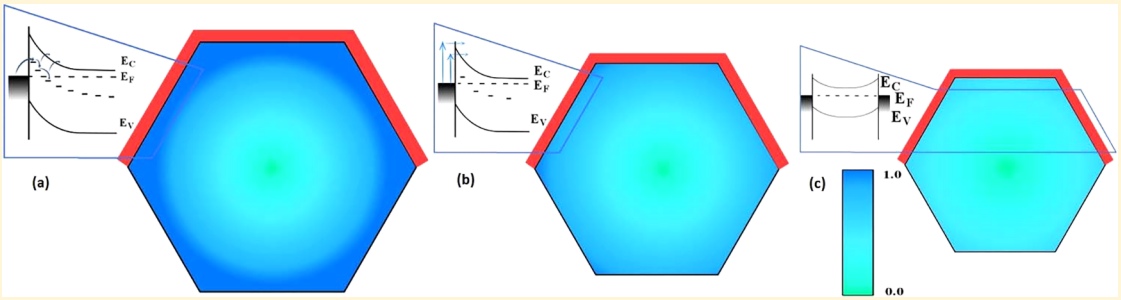

ABSTRACT: Surface states that induce depletion regions are commonly believed to control the transport of charged carriers through semiconductor nanowires. However, direct, localized optical, and electrical measurements of ZnO nanowires show that native point defects inside the nanowire bulk and created at metal−semiconductor interfaces are electrically active and play a dominant role electronically, altering the semiconductor doping, the carrier density along the wire length, and the injection of charge into the wire. We used depth-resolved cathodoluminescence spectroscopy to measure the densities of multiple point defects inside ZnO nanowires, substitutional Cu on Zn sites, zinc vacancy, and oxygen vacancy defects, showing that their densities varied strongly both radially and lengthwise for tapered wires. These defect profiles and their variation with wire diameter produce trap-assisted tunneling and acceptor trapping of free carriers, the balance of which determines the low contact resistivity (2.6×10^{-3} $\Omega \cdot cm^{-2}$) ohmic, Schottky ($\Phi \geq 0.35$ eV) or blocking nature of Pt contacts to a single nano/microwire. We show how these defects can now be manipulated by ion beam methods and nanowire design, opening new avenues to control nanowire charge injection and transport.

KEYWORDS: *ZnO, nanowire, defect, ohmic, Schottky contact, cathodoluminescence spectroscopy*

Electrical contacts to semiconductor nanowires are integral to a wide range of device applications,[1−7] yet they exhibit electronic properties that depend strongly on their physical size. For metal interfaces to bulk semiconductors, the nature of charge transfer and barrier formation depend sensitively on the chemical, geometrical, and electronic structure at their intimate junction.[8,9] For metal interfaces to semiconductor nanowires, the scale and physical geometry of these junctions introduces additional and unique features including three-dimensional depletion regions and space charge limited injection.[2,10] The high surface-to-volume nature of these nano- and microwires amplifies these effects of local band bending, the resultant free carrier depletion within wires,[11] and their dependence on ambient effects.[12−15] Electrically active defects at surfaces also can control carrier transport lengthwise inside nanowires by adsorbate-induced charging that alters depletion regions radially. These defects are present inside as well as at the surfaces of nano- and microwires.[16] Their presence has been inferred from electrical[17−21] and optical[22,23] measurements of devices and their interfaces but direct localized measurements correlating them with electronic contact behavior have not until now been available. We have now measured these defects inside ZnO nano/microwires and at their metal interfaces to show how the physical nature, density, and spatial distribution of these defects dominates the Schottky, ohmic, or blocking behavior of these contacts.

We used depth-resolved cathodoluminescence spectroscopy (DRCLS)[24] to measure defect type, density, and spatial distributions, inside the "bulk" of single nano/microwires and

Received: July 16, 2018
Revised: October 31, 2018
Published: November 1, 2018

DOI: 10.1021/acs.nanolett.8b02892
Nano Lett. 2018, 18, 6974−6980

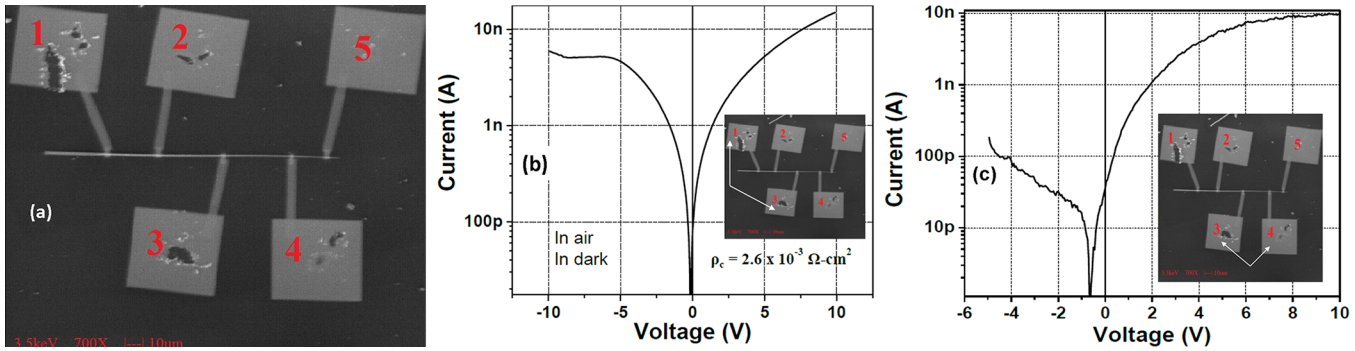

Figure 1. (a) Tapered ZnO nanowire with five Pt contact and wire pads. (b) *I*−*V* characteristics in dark and in air between Contacts 1 and 3 versus (c) 3 and 4. The insets within (b,c) display the secondary electron image (SEI) of the contact with arrows to indicate the probe locations.

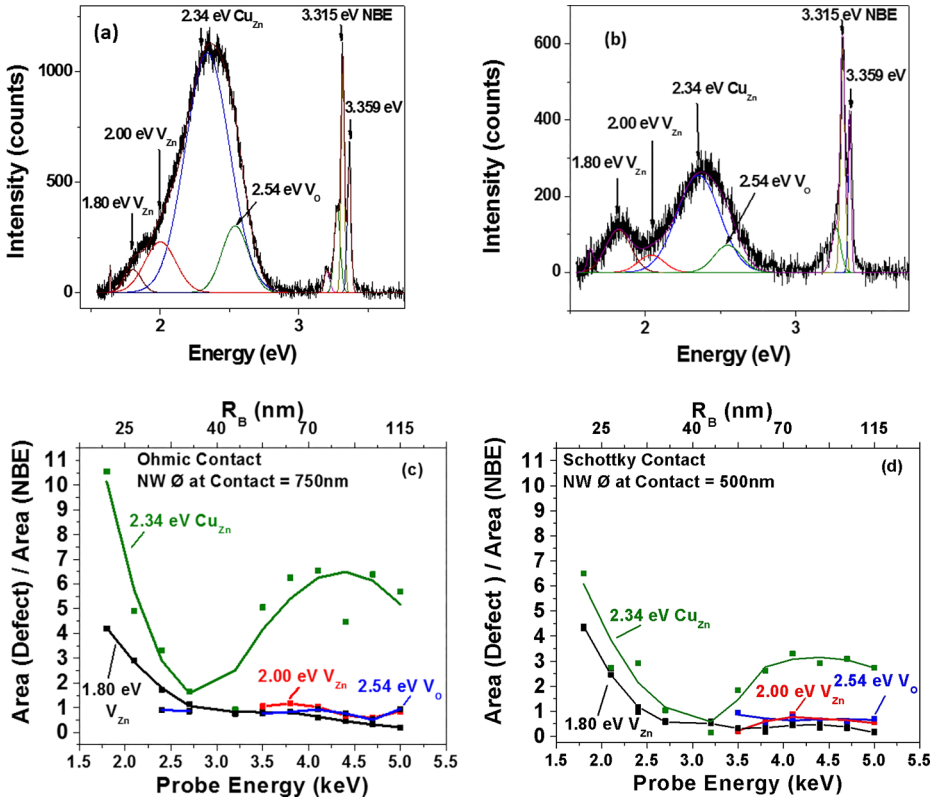

Figure 2. DRCL spectra at E_B = 5.0 keV at (a) Ohmic Contact 3 and (b) Schottky Contact 4 with defect peak Gaussian deconvolutions. The 2.35 eV Cu_{Zn} defect decreases significantly at Contact 4. Depth profiles of deconvolved defect areas for (c) Contact 3 and (d) Contact 4, both showing pronounced minima at about 50 nm depth and surface segregation, 2 times stronger for ohmic Contact 3.

their interfaces with the same Pt metal, whose Schottky and ohmic contacts have been studied previously.[25−28] Using E_B = 0.5−5 keV incident beam energies, one can achieve near-nanometer depth resolution through bare surfaces as well as through thin metal contact layers.[29] Monte Carlo simulations provided profiles of energy-dependent excitation depths in good agreement with experimental measurements.[30] For bare ZnO surfaces and E_B = 0.5−3 keV, peak electron−hole pair creation rates ranged from U_0 = 1.5 to 22 nm with maximum excitation (Bohr−Bethe) range R_B = 18−76 nm, respectively. See Supplementary Figure S1. Simulations show that these depths are reduced significantly depending on thickness and atomic density for excitation through metal overlayers. Nevertheless, excitation through 20−30 nm thick metal overlayers produces luminescence at the semiconductor interface that can pass back through the metal and be collected by an optical train. DRCLS coupled with the 5−10 nm incident beam spot size of our UHV-scanning electron microscope (SEM) provided near-nm scale spatial resolution in three dimensions.

The ability to measure spatially localized luminescence inside ZnO nanowires and at their metal interfaces enabled us to address several questions: (i) what is the nature and distribution of native point defects at nanostructures' interfaces; (ii) what effect do these defects have on interface electronic properties; and (iii) can the nature and spatial distribution of these defects be controlled. To address all three issues, we performed DRCLS and current−voltage (*I*−*V*) measurements on ZnO nano- and microwires of varying diameters and with Pt contacts to the same nano/microwire. Figure 1 illustrates a ZnO nanowire grown by a carbo-thermal technique.[31] Figure 1a shows the pattern of Pt wire contacts

DOI: 10.1021/acs.nanolett.8b02892
Nano Lett. 2018, 18, 6974−6980

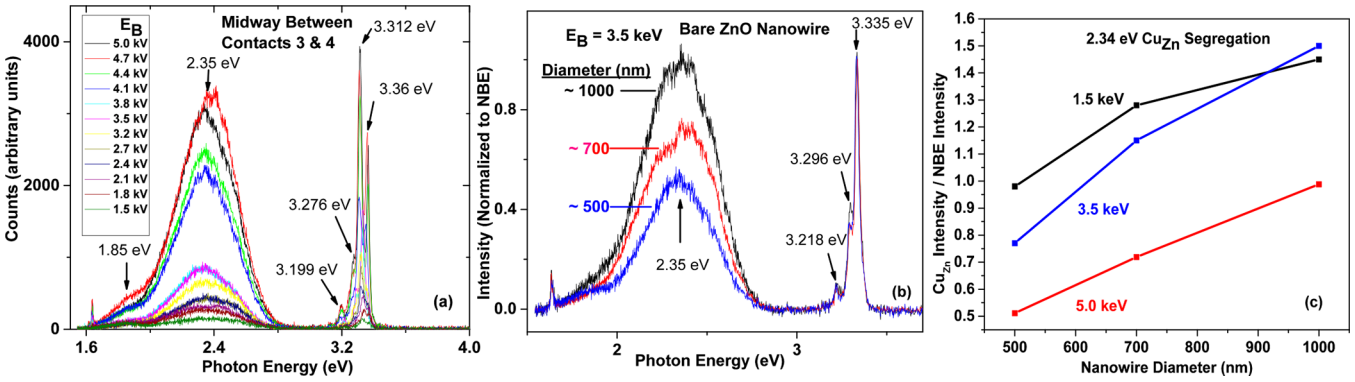

Figure 3. (a) The 80 K DRCLS deep level defect emissions below ZnO band gap energy versus E_B midway between Contacts 3 and 4. (b) The 3.5 keV DRCL spectra normalized to band gap intensity at three wire diameters. (c) The 2.35 eV defect intensities versus wire diameter for three E_B and excitation depths showing Cu_{Zn} increase with increasing diameter at all depths.

across a 60 μm long nanowire whose diameter varied linearly from 400 nm to 1 μm. Even with the same metal contacting the same nanowire, these five contacts exhibited a wide range of contact behavior. Pt contacts to 10 other carbothermal and pulsed laser-deposited (PLD) nanowires exhibited analogous behavior. Figure 1b exhibits nearly ohmic $I-V$ behavior between Contacts 1 and 3, indicating that both contacts are ohmic in nature. Figure 1c exhibits Schottky behavior with reverse current at −6 V bias, 2 orders of magnitude lower than in forward bias (+6 V). Note the zero bias voltage offset characteristic of a built-in voltage at an insulating interface.[32] Ohmic behavior between Contacts 1 and 3 versus Schottky behavior between Contacts 3 and 4 shows that Contacts 1, 3, and 4 were ohmic, ohmic, and rectifying, respectively.

Contact 2 did not pass current, indicating a break in the deposited Pt leading on to the ZnO surface. Contact 5 was blocking. In general, electrical contact measurements to these nanowires yielded ohmic (blocking) contacts to high (low) defect density regions. Only three contacts to nine wires exhibited Schottky behavior with an average $\Phi_{SB} = 0.40 \pm 0.16$ eV. This is understandable since only tapered wire regions with low defect density to minimize tunneling but high enough to prevent blocking exhibited rectification, and those regions could be located only by first measuring their spatially varying defect densities. The fitting procedure used to extract Φ_{SB} consisted of extrapolating the forward bias $I-V$ slope to zero applied voltage and using the $J_0 = A^{**}T^2 \exp(-q\Phi_{SB}/kT)$ relationship to extract Φ_{SB}.

Figure 2 compares cathodoluminescence (CL) spectra of Contact 3 versus 4 to show the local differences in defects at their interfaces that can account for the ohmic versus Schottky $I-V$ characteristics, respectively, in Figure 1. Here the incident electron beam on the Pt contact overlaps the Pt contact edges to excite the nanowire closest to the Pt−ZnO interface. Figure 2a,b spectra exhibit deconvolved components corresponding to the band gap (3.359 eV), a near-band edge exciton (3.315 eV), zinc vacancy (V_{Zn}) and vacancy clusters (1.80 and 2.0 eV, respectively), and copper on zinc site (Cu_{Zn}) substitutionals (2.34 eV) that have been identified previously.[33] The relative intensities and deconvolved areas of these features vary with excitation depth and with position along the wire length. See Supporting Information Figures S2 and S3, respectively. Figure 2a shows a 2.34 eV Cu_{Zn} defect emission that dominates all other features, whereas this feature is significantly lower in Figure 2b. Figure 2c plots the ratio of integrated areas of all the deconvolved defects shown in Figure 2a versus the near band edge (NBE) area as a function of E_B and R_B. The integrated area for the Cu_{Zn} peak feature normalized to the NBE peak area $A(Cu_{Zn})/A(NBE)$ shows a nearly 10 times increase toward the surface, nearly double the ratio deep inside the wire. $A(V_{Zn})/A(NBE)$ for the 1.8 eV V_{Zn} emission shows a similar increase toward the surface while the 2.0 eV $A(V_{Zn})/A(NBE)$ and 2.54 eV $A(V_O)/A(NBE)$ ratios remain relatively low. Figure 2d shows the corresponding profile for Schottky Contact 4. Similar to Figure 2c, pronounced Cu_{Zn} and V_{Zn} segregation is evident but reduced for Cu_{Zn} by 2 times toward the surface and 10 times at its minimum. Bulk ratios for all four defects are >2 times smaller for Contact 4 versus Contact 3 as well as midway between Contacts 3 and 4. See Supporting Information Figure S3. Pronounced Cu_{Zn} minima are evident in Figure 2c,d at ∼35−45 nm below the nanowire surface. Similar Cu_{Zn} minima are evident for metal contacts to bulk ZnO Zn- and O-polar crystals, attributed to electric field-driven diffusion of these acceptor defects within the surface space charge region of the contact.[34]

The lower defect densities at Contact 4 can be attributed to a monotonic decrease in bulk and segregated Cu_{Zn} with decreasing wire diameter. Figure 3a shows representative spectra obtained at 80 K of the bare ZnO nanowire midway between Contacts 3 and 4. Near band edge (NBE) features at 3.36, 3.312, 3.276, and 3.199 eV correspond to free exciton, donor-bound exciton, and two phonon replicas, respectively,[35] while the 2.35 and 1.85 eV features again correspond to Cu_{Zn} and V_{Zn} sites, respectively. Figure 3b shows Cu_{Zn} peak intensity for E_B = 3.5 keV, corresponding to ∼80 nm excitation depth within the wire for different diameters. Based on a previous NBE-normalized calibration,[36] near-surface V_{Zn} densities are estimated to be $\sim 1 \times 10^{21}$ cm^{-3}. However, calibration of Cu_{Zn} densities is not yet available. Supporting Information includes Table S1 showing correlations between defect intensities and wire diameter in common for 10 different nano- and microwires grown by multiple techniques.

Both carbothermal and PLD-grown ZnO nanowires exhibit tapering. Tapering occurs in homogeneous ZnO wires, probably due to growth kinetics and possibly slightly inhomogeneous growth conditions. It is not unique to a particular growth method nor to any core−shell structure. Tapering in the wires studied here is mild, whereas it can be strong toward the tip of standing wires.[37]

Using our focused electron beam with nanoscale depth control, we were able to excite only the nanowire and not the underlying SiO_2/Si substrate. Figure S4 illustrates a DRCL

DOI: 10.1021/acs.nanolett.8b02892
Nano Lett. 2018, 18, 6974−6980

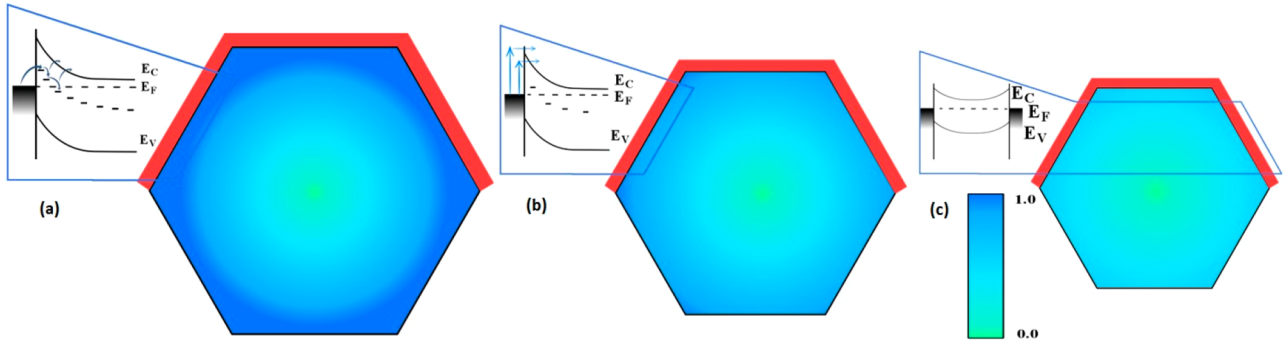

Figure 4. Schematic diagrams of band bending at Pt-ZnO nano/microwire contact for (a) 900 nm, (b) 600 nm, and (c) 400 nm diameter wires linked to the interfaces of their corresponding wires. Darker shading signifies higher acceptor density and defect-assisted hopping with increasing radius. With decreasing diameter, interface acceptor density decreases and contact behavior changes from transport by (a) trap-assisted tunneling to (b) Schottky rectification to (c) blocking regions extending radially from multiple faceted surfaces can almost fully deplete the 400 nm diameter nanowire.

spectrum of a SiO_2/Si substrate supporting these ZnO nanowires. The pronounced 1.91 eV peak is characteristic of nonbonding oxygen hole center (NBOHC) defects,[38] which are completely absent from spectra in Figures 2 and S2. Another common SiO_2 defect termed E' frequently present in SiO_2 occurs at 2.7 eV[23,39] but is also not present in these spectra. Pt metal overlayers also do not contribute to the observed luminescence.

The densities and spatial distributions of V_{Zn} and Cu_{Zn} defects inside the ZnO nanowire and their monotonic decrease with decreasing wire diameter can explain the striking difference in their measured contact properties. The ohmic $I-V$ characteristics of Contacts 1 and 3 in Figure 1b can be interpreted as trap-assisted hopping transport since the spatial separation of these defects is comparable to their wave function overlap. Assuming a hydrogenic model,[40] the wave function extent a for the V_{Zn} trap can be expressed as $a = \hbar/(2m^*E_t)^{1/2}$ where the ZnO effective mass $m^* = 0.30\ m_0$ so that for trap depth E_t = 3.365−2.54 = 0.83 eV below the conduction band, a = 3.90 Å. For the Cu_{Zn} trap with E_t = 3.365−2.35 = 1.015 eV, a = 3.53 Å. On the basis of the previous calibration for V_{Zn},[34] and the normalized V_{Zn} amplitude in Figure 2, $[V_{Zn}] = 1.17 \times 10^{21}$ cm^{-3} midway between Contacts 3 and 4. Assuming that $[Cu_{Zn}]$ and $[V_{Zn}]$ densities are comparable, then their combined density is $N_t = 2.3 \times 10^{21}$ cm^{-3} and their spatial separation R is obtained from $4\pi/3R^3 = (1/N_t)$ or R = 4.7 Å. Hence, the spatial separation of trap states is comparable to the wave function extent, suggesting significant wave function overlap and trap-assisted hopping. Note that $[Cu_{Zn}]$ is even higher for Contacts 1 and 3 based on NBE-normalized areas in Figure 3c. The Schottky barrier $I-V$ characteristic for Contact 4 appears to reflect the 2 times decrease in segregated Cu_{Zn} in Figure 3c,d, which translates to a 30% increase in spatial separation. Note that residual hopping may contribute to the relatively low Schottky barrier Φ_{SB} = 0.35 eV compared with literature values[41] as well as carbon incorporation in the EBID Pt contacts. Finally, the blocking contact measured for Contact 5 is consistent with the depletion layer width now comparable or greater than the nanowire radius.[11] Previous resistivity measurements of similar ZnO nanowires suggest nominally undoped carrier densities $n = 1-3 \times 10^{17}$ cm^{-3}.[13] With compensating V_{Zn} and Cu_{Zn} acceptors reported here, resultant carrier density N should decrease significantly below 10^{17} cm^{-3}. Together with a V_0 = 0.35 eV barrier height, a 10^{16} cm^{-3} net electron density, and dielectric constant $\varepsilon = 8.75\ m_o$, the Pt−ZnO depletion width $W = [2\varepsilon V_0/qN]^{1/2}$ = 206 nm so that depletion extends well into the nanowire from the three contacted facets.

Figure 4 illustrates schematic cross sections of the wire at diameters comparable to Contacts 1, 4, and 5, showing the band bending and proposed charge transport across their interfaces for each. Figure 4a depicts trap-assisted transport through the high defect density band bending region. Figure 4b shows both thermionic emission and trap-assisted tunneling, whereas Figure 4c illustrates band bending regions extending from opposite faces that fully deplete the nanowire interior. Figure 4 is a schematic representation of how the defect depth profiles look and how they explain the phenomenological behavior observed. Software such as Sentaurus can define the geometry of the model, a radially varying defect density, then calculate and draw the corresponding band profile to the metal contact. Overall, monotonic variation of (i) native point defect density versus wire diameter, (ii) defect-assisted hopping across the depletion region, (iii) compensation of electron density by these deep level acceptors, and (iv) "pinch-off" of carrier density in the wire core for the narrowest wire diameters can account for the wide variation in metal-nanowire interface behavior.

Temperature-dependent $I-V$ characteristics support the proposed trap-assisted tunneling. In Supporting Information Figure S5, Schottky-like behavior is evident between milled and Ga-implanted (ohmic) contacts whereas more ohmic behavior appears between unmilled and Ga-implanted contacts. For all three combinations, forward current is reduced by 10^2 X between T = 300 and 80 K, consistent with conventional $J_0 = A^{**}T^2 \exp(-q\Phi_{SB}/kT)$ Schottky behavior whereas reverse current is reduced by $>10^4$ X, suggesting a reduction in thermally activation hopping conduction. Note also that the milled-to-Ga-implanted contacts exhibit Schottky-like behavior in contrast to the unmilled-to-Ga-implanted contacts.

We observed variability in ohmic contact resistivity, which can be due to numerous factors including variations in defect density and distribution, interface reactivity, interface contamination, as well as work function differences.[42] However, for the same metal on the same semiconductor prepared in the same high vacuum chamber by the same deposition method, all but defect density, donor/acceptor nature, and resultant doping are the same. Since nanowire doping and defects can vary between different nanowires,[43] meaningful isolation of

DOI: 10.1021/acs.nanolett.8b02892
Nano Lett. 2018, 18, 6974−6980

defect density and doping must involve comparison of contacts strictly within the same nanowire as shown here.

The dependence of contact properties on native point defects inside as well as at the surface of these ZnO nanowires indicates the value of controlling defect densities in nanowires after growth. For example, it is possible to remove high concentrations of segregated defects, such as those within the outer 40−50 nm annulus shown in Figures 2c,d, by ion milling. Figure 5a shows an SEI of a 700 nm diameter wire which is

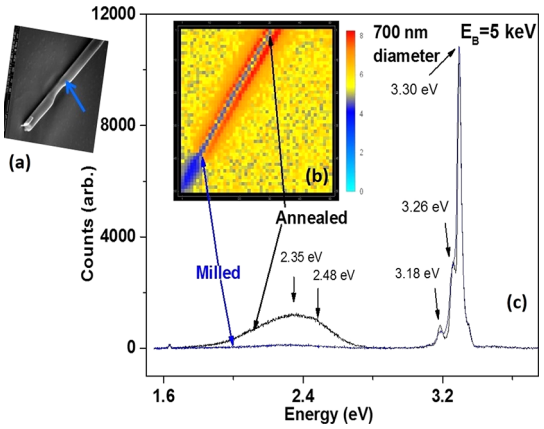

Figure 5. (a) SEI, (b) HSI, and (c) E_B = 5 keV CL spectra of 5 keV Ga^+ milled removal of segregated defects in outer annulus versus e-beam annealed defect increase in contiguous regions of a 700 nm ZnO wire on SiO_2. HSI color gradient signifies magnitude of integrated 1.5−2.75 eV defect areas normalized by NBE integrated area. Defects increase from milled wire section toward annealed region.

reduced to 400 nm by 5 kV Ga^+ milling. The corresponding hyperspectral image of this wire in Figure 5b shows that the 1.5−2.75 eV integrated area of NBE-normalized defect emission decreases at the milled portion of the wire (lower left).

In contrast, electron beam heating increases defect densities in a nearby length of wire (upper right). The E_B = 5 keV CL spectra in Figure 5c shows more than an order of magnitude decrease in defect emission due to milling compared with increased defect emissions due to local heating. The electron beam conditions used for DRCLS are 2 orders of magnitude lower power density than the electron beam used to anneal the wire in Figure 5, an order of magnitude lower current and an order of magnitude lower voltage. Consistent with little or no heating, the spectra show little or no change in near band edge luminescence, whereas heating of more than ∼10 °C would shift the band gap emission to measurably lower energies, a red shift that is not observed. Likewise, the CL spectra show no change in the defect emissions with repeated measurements of the same area over time, consistent with no observable damage. Nearly the same thermal conductivity between ZnO[44] and Si[45] nanowires as well as the higher thermal conductivities of GaN[1] and SiC[46] suggest similar thermal behavior.

The ion milling itself adds negligible defects since the 5 keV Ga ions have a projected range R_p of only 4.4 nm compared with the 300 nm diameter reduction. By comparison, Supporting Information Figure S6 shows that a commonly used 30 keV Ga beam's range is ∼3 times larger. Supporting Information Figure S5 shows that a milled-to Ga-implanted contacts exhibit Schottky-like behavior in contrast to the unmilled-to-Ga-implanted contacts. This demonstrates that defect density in nanostructures can control contact behavior. Figure 5 shows that low energy Ga milling can reduce native defects in ZnO nanowires substantially. Combined with focused electron beam heating, it is possible to engineer orders of magnitude variation in defect density over distances of only a few microns.

In summary, these results illustrate how native point defects in nanowires can vary spatially both radially and lengthwise, either as they are grown or as they are locally milled or heated. As previously reported, these defects can be present throughout the nanowires with densities and nature that depend on growth method. As shown here, these spatial variations are different for different defects within the same ZnO nanostructure. The electrical contact properties of a single ZnO nanowire grown by a carbo-thermal method are found to depend on the density and spatial distribution of Cu_{Zn} and V_{Zn} acceptor defects inside nano- and microwires measured by DRCLS, resulting in ohmic, Schottky, or blocking contacts for the same metal on the same ZnO nanowire. The DRCLS approach described here has the potential for application to other materials. Indeed, the ability to obtain CL spectra of individual nanowires at low kV beam energies comparable to those used here without apparent damage is evident in InP,[47] InAs,[48] and GaAs[49] studies.

■ ASSOCIATED CONTENT

Supporting Information

The Supporting Information is available free of charge on the ACS Publications website at DOI: 10.1021/acs.nanolett.8b02892.

Monte Carlo distributions of e-h pair creation versus depth and incident beam energy, DRCL spectra of bare ZnO wires between contacts and in depth, table of ZnO wire defect−NBE intensity ratio versus wire diameter, temperature-dependent $I-V$ characteristics of milled, unmilled, and Ga-implanted contacts, DRCLS spectra of SiO_2/Si substrate under wires, and SRIM simulations of accelerated Ga ions in ZnO (PDF)

■ AUTHOR INFORMATION

Corresponding Author

*E-mail: brillson.1@osu.edu.

ORCID

Leonard J. Brillson: 0000-0003-3527-9761

Author Contributions

L.J.B. conceived the experiment and coordinated the research work with the help of J.C., G.F., and A.J. J.C. and A.F. performed the electronic and microscopic characterization. H.v.W. and M.G. performed the growth. J.C. and L.J.B. wrote the paper.

Notes

The authors declare no competing financial interest.

■ ACKNOWLEDGMENTS

The authors gratefully acknowledge National Science Foundation, Grant DMR-1800130 and Deutsche Forschungsgemeinschaft (Gr 1011/26- 1) for support of this work.

DOI: 10.1021/acs.nanolett.8b02892
Nano Lett. 2018, 18, 6974−6980

REFERENCES

(1) Schmidt-Mende, L.; MacManus-Driscoll, J. L. *Mater. Today* **2007**, *10*, 40−48.
(2) Léonard, F.; Talin, A. A. *Nat. Nanotechnol.* **2011**, *6*, 773−783.
(3) Zekentes, K.; Rogdakis, K. *J. Phys. D: Appl. Phys.* **2011**, *44*, 133001.
(4) English, C. D.; Shine, G.; Dorgan, V. E.; Saraswat, K. C.; Pop, E. *Nano Lett.* **2016**, *16*, 3824−3830.
(5) Dasgupta, N. P.; Yang, P. *Front. Phys.* **2014**, *9*, 289−302.
(6) Agarwal, R. *Small* **2008**, *4*, 1872−1893.
(7) Sato, K.; Castaldini, A.; Fukata, N.; Cavallini, A. *Nano Lett.* **2012**, *12*, 3012−3017.
(8) Brillson, L. J. *Surf. Sci. Rep.* **1982**, *2*, 123−326.
(9) Brillson, L. J. *Surfaces and Interfaces of Electronic Materials*; Wiley-VCH, 2010.
(10) Léonard, F.; Talin, A. A. *Phys. Rev. Lett.* **2006**, *97*, 026804.
(11) Bercu, B.; Geng, W.; Simonetti, O.; Kostcheev, S.; Sartel, C.; Sallet, V.; Lérondel, G.; Molinari, M.; Giraudet, L.; Couteau, C. *Nanotechnology* **2013**, *24*, 415202.
(12) Goldberger, J.; Sirbuly, D. J.; Law, M.; Yang, P. ZnO Nanowire Transistors. *J. Phys. Chem. B* **2005**, *109*, 9−14.
(13) Zimmermann, G.; Lange, M.; Cao, B.; Lorenz, M.; Grundmann, M. Resistivity control of ZnO nanowires by Al doping. *Phys. Status Solidi RRL* **2010**, *4*, 82−84.
(14) Schlenker, E.; Bakin, A.; Weimann, T.; Hinze, P.; Weber, D. H.; Gölzhäuser, A.; Wehmann, H.-H.; Waag, A. *Nanotechnology* **2008**, *19*, 365707.
(15) Lao, C. S.; Liu, J.; Gao, P.; Zhang, L.; Davidovic, D.; Tummala, R.; Wang, Z. L. ZnO Nanobelt/nanowire Schottky Diodes Formed by Dielectrophoresis Alignment across Au Electrodes. *Nano Lett.* **2006**, *6*, 263−266.
(16) Ruane, W. T.; Leedy, K.; Look, D. C.; Farlow, G.; von Wenckstern, H.; Grundmann, M.; Brillson, L. J. Defect Segregation and Optical Emission in ZnO Nanowires and Microwires. *Nanoscale* **2016**, *8*, 7631−7637.
(17) Hong, W.-K.; Sohn, J. I.; Hwang, D.-K.; Kwon, S.-S.; Jo, G.; Song, S.; Kim, S.-M.; Ko, H.-J.; Park, S.-Ju.; Welland, M. E.; Lee, T. Tunable Electronic Transport Characteristics of Surface-Architecture-Controlled ZnO Nanowire Field Effect Transistors. *Nano Lett.* **2008**, *8*, 950−956.
(18) Li, P.; Liao, Q.; Zhang, Z.; Wang, Z.; Lin, P.; Zhang, X.; Kang, Z.; Huang, Y.; Gu, Y.; Yan, X.; Zhang, Y. Investigation on the Mechanism of Nanodamage and Nanofailure for Single ZnO Nanowires under an Electric Field. *ACS Appl. Mater. Interfaces* **2014**, *6*, 2344−2349.
(19) Shao, Z. Z.; Zhang, Z. A.; Wang, Z. F.; Chang, S. L. Electrical characteristics of Pt-ZnO Schottky nano-contact. *Sci. China: Phys., Mech. Astron.* **2010**, *53*, 64−67.
(20) Weissenberger, D.; Gerthsen, D.; Reiser, A.; Prinz, G. M.; Feneberg, M.; Thonke, K.; Zhou, H.; Sartor, J.; Fallert, J.; Klingshim, C.; Kalt, H. Influence of the measurement procedure on the field-effect dependent conductivity of ZnO nanorods. *Appl. Phys. Lett.* **2009**, *94*, 042107.
(21) Lee, T. I.; Choi, W. J.; Kar, J. P.; Kang, Y. H.; Jeon, H. H.; Park, J. H.; Kim, Y. S.; Baik, H. K.; Myoung, J. M. Electrical Contact Tunable Direct Printing Route for a ZnO Nanowire Schottky Diode. *Nano Lett.* **2010**, *10*, 3517−3523.
(22) Djurišič, A. B.; Leung, Y. H. Optical Properties of ZnO Nanostructures. *Small* **2006**, *2*, 944−961.
(23) Oh, Y. M.; Lee, K. M.; Park, K. H.; Kim, Y.; Ahn, Y. H.; Park, J.-Y.; Lee, S. Correlating Luminescence from Individual ZnO Nanostructures with Electronic Transport Characteristics. *Nano Lett.* **2007**, *7*, 3681−3685.
(24) Brillson, L. J. Applications of Depth-Resolved Cathodoluminescence Spectroscopy. *J. Phys. D: Appl. Phys.* **2012**, *45*, 183001−183027.
(25) Heo, Y. W.; Tien, L. C.; Norton, D. P.; Pearton, S. J.; Kang, B. S.; Ren, F.; LaRoche, J. R. Pt/ZnO nanowire Schottky diodes. *Appl. Phys. Lett.* **2004**, *85*, 3107.
(26) He, J.-H.; Ke, J.-J.; Chang, P.-H.; Tsai, K.-T.; Yang, P. C.; Chan, I.-M. Development of Ohmic nanocontacts via surface modification for nanowire-based electronic and optoelectronic devices: ZnO nanowires as an example. *Nanoscale* **2012**, *4*, 3399.
(27) Das, S. N.; Kar, J. P.; Myoung, J.-M. Junction Properties and Applications of ZnO Single Nanowire Based Schottky Diode. In *Nanowires-Fundamental Research*; Hashim, A., Ed.; InTech, 2011.
(28) Mao, S.; Shang, T.; Park, B.; Anderson, D. D.; Dillon, S. J. *Appl. Phys. Lett.* **2014**, *104*, 153105.
(29) Asel, T. J.; Gao, H.; Heinl, T. J.; Adkins, D.; Woodward, P. M.; Hoffman, J.; Bhattacharya, A.; Brillson, L. J. Near-Nanoscale-Resolved Energy Band Structure of $LaNiO_3/La_{2/3}Sr_{1/3}MnO_3/SrTiO_3$ Heterostructures and their Interfaces. *J. Vac. Sci. Technol., B: Nanotechnol. Microelectron.: Mater., Process., Meas., Phenom.* **2015**, *33*, 04E103.
(30) Drouin, D. CASINO a Powerful Simulation Tool for Cathodoluminescence Applications. *Microsc. Microanal.* **2006**, *12*, 1512.
(31) Dietrich, C. P.; Brandt, M.; Lange, M.; Kupper, J.; Böntgen, T.; von Wenckstern, H.; Grundmann, M. Defect properties of ZnO and ZnO:P microwires. *J. Appl. Phys.* **2011**, *109*, 013712.
(32) Mosbacker, H. L.; Zgrabik, C.; Hetzer, M. J.; Swain, A.; Look, D. C.; Cantwell, G.; Zhang, J.; Song, J. J.; Brillson, L. J. Thermally driven defect formation and blocking layer at metal-ZnO interfaces. *Appl. Phys. Lett.* **2007**, *91*, 072102.
(33) Brillson, L. J.; Ruane, W. T.; Gao, H.; Zhang, Y.; Luo, J.; von Wenckstern, H.; Grundmann, M. Spatially-Resolved Cathodoluminescence Spectroscopy of ZnO Defects; *Materials Science in Semiconductor Processing*; Elsevier, 2016; Vol. *57*, 197−209 and references therein.
(34) Foster, G. M.; Gao, H.; Mackessy, G.; Hyland, H. M.; Allen, M. W.; Wang, B.; Look, D. C.; Brillson, L. J. Impact of defect distribution on IrO_x/ZnO interface doping and Schotty barriers. *Appl. Phys. Lett.* **2017**, *111*, 101604.
(35) Meyer, B. K.; Alves, H.; Hofmann, D. M.; Kriegseis, W.; Forster, D.; Bertram, F.; Christen, J.; Hoffmann, A.; Straβburg, M.; Dworzak, M.; Haboeck, U.; Rodina, A. V. Bound exciton and donor-acceptor pair recombination in ZnO. *Phys. Status Solidi B* **2004**, *241*, 231−260.
(36) Foster, G. M.; Faber, G.; Yao, Y.-F.; Yang, C. C.; Heller, E. R.; Look, D. C.; Brillson, L. J. Direct measurement of defect and dopant abruptness at high electron mobility ZnO homojunctions. *Appl. Phys. Lett.* **2016**, *109*, 143506.
(37) Nobis, T.; Kaidashev, E. M.; Rahm, A.; Lorenz, M.; Grundmann, M. Whispering Gallery Modes in Nanosized Dielectric Resonators with Hexagonal Cross Sections. *Phys. Rev. Lett.* **2004**, *93*, 103903.
(38) Kalceff, M. A.; Phillips, M. R. Cathodoluminescence microcharacterization of the defect structure of quartz. *Phys. Rev. B: Condens. Matter Mater. Phys.* **1995**, *52*, 3122−3135.
(39) White, B. D.; Brillson, L. J.; Bataiev, M.; Fleetwood, D. M.; Schrimpf, R. D.; Choi, B. K.; Pantelides, S. T. Detection of trap activation by ionizing radiation in SiO_2 by spatially localized cathodoluminescence spectroscopy. *J. Appl. Phys.* **2002**, *92*, 5729−5734.
(40) Look, D. C.; Walters, D. C.; Manasreh, M. O.; Sizelove, J. R.; Stutz, C. E.; Evans, K. R. Anomalous Hall-effect results in low-temperature molecular-beam-epitaxial GaAs: Hopping in a dense EL2-like band. *Phys. Rev. B: Condens. Matter Mater. Phys.* **1990**, *42*, 3578−3581.
(41) Brillson, L. J.; Lu, Y. ZnO Schottky Barriers and Ohmic Contacts. *J. Appl. Phys.* **2011**, *109*, 121301.
(42) For example, Brillson, L.J. *Surfaces and Interfaces of Electronic Materials*; Wiley-VCH: Weinheim, 2010.
(43) Brillson, L. J.; Ruane, W.T.; Gao, H.; Zhang, Y.; Luo, J.; von Wenckstern, H.; Grundmann, M. Spatially-Resolved Cathodoluminescence Spectroscopy of ZnO Defects. *Materials Science in Semiconductor Processing*; Elsevier, 2016; Vol. *57*, pp 197−209.
(44) Wu, X.; Lee, J.; Varshney, V.; Wohlwend, J. L.; Roy, A.; Luo, T. Thermal Conductivity of Wurtzite Zinc-Oxide from First-Principles

DOI: 10.1021/acs.nanolett.8b02892
Nano Lett. 2018, 18, 6974−6980

Lattice Dynamics - a Comparative Study with Gallium Nitride. *Sci. Rep.* **2016**, *6*, 22504−22513.
(45) Hochbaum, A. I.; Chen, R.; Delgado, R. D.; Liang, W.; Garnett, E. C.; Najarian, M.; Majumdar, A.; Yang, P. Enhanced thermoelectric performance of rough silicon nanowires. *Nature* **2008**, *451*, 163−167.
(46) Zhu, B.; Wang, R.; Harrison, S.; Williams, K.; Goduguchinta, R.; Schneiter, J.; Pegna, J.; Vaaler; Wang, X. Thermal conductivity of SiC microwires: Effect of temperature and structural domain size uncovered by 0 K limit phonon scattering. *Ceram. Int.* **2018**, *44*, 11218−11224.
(47) Storm, K.; Halvardsson, F.; Heurlin, M.; Lindgren, D.; Gustafsson, A.; Wu, P. M.; Monemar, B.; Samuelson, L. Spatially resolved Hall effect measurement in a single semiconductor nanowire. *Nat. Nanotechnol.* **2012**, *7*, 718−722.
(48) Zhang, G.; Tateno, K.; Sogawa, T.; Gotoh, H. Diameter-tailored telecom-band luminescence in InP/InAs heterostructure nanowires grown on InP (111)B substrate with continuously-modulated diameter from microscale to nanoscale. *Nanotechnology* **2018**, *29*, 155202−12.
(49) Sedrine, N. B.; Ribeiro-Andrade, R.; Gustafsson, A.; Soares, M. R.; Bourgard, J.; Teixeira, J. P.; Salomé, P. M. P.; Correia, M. R.; Moreira, M. V. B.; De Oliveira, A. G.; González, J. C.; Leitão. Fluctuating potentials in GaSi:Si nanowires: critical reduction of the influence of polytypism on the electronic structure. *Nanoscale* **2018**, *10*, 3697−3708.

DOI: 10.1021/acs.nanolett.8b02892
Nano Lett. 2018, 18, 6974−6980